Density Functional Theory of Phase Transitions in Diblock Copolymer Systems

Robert L. Lescanec† and M. Muthukumar*

Polymer Science and Engineering Department and Materials Research Laboratory, University of Massachusetts, Amherst, Massachusetts 01003

Received November 16, 1992; Revised Manuscript Received February 26, 1993

ABSTRACT: We present a general theoretical scheme which allows the characterization of microphase separation of A–B diblock copolymer systems at *all* degrees of segregation. Our method is based on the density functional theory of Melenkevitz and Muthukumar and uses the technique of density profile parameterization to greatly reduce the technical complexity of the solution. The microphase-separated systems are observed to pass through three stages of ordering as the system is quenched. These are the weak, intermediate, and strong segregation regimes. The phase diagram is calculated for three ordered morphologies: lamellae, hexagonally-packed cylinders, and body-centered-cubic spheres. We also characterize these microphases by the dependence of the lattice constant, D, and the interfacial width, σ_0, on the quench parameter χN. The theory correctly reproduces the behavior predicted by previous theories describing the weak and strong segregation regimes and establishes the experimental conditions for the validity of these regimes. In the intermediate regime, the effective exponent α describing the N dependence of D ($D \approx N^{\alpha}$) is larger than that in the strong segregation regime. α depends strongly on both block length and morphology in the intermediate regime. We attribute this behavior to chain stretching arising from the localization of junctions.

Introduction

During the last two decades several theories were developed attempting to characterize the physical phenomena associated with the ordering of A–B diblock copolymers upon microphase separation.[1] However, investigation of the phase diagram was restricted to very specific regimes of microphase separation due to the formalisms employed and inherent assumptions present in these theories. These developments concentrated on either the weak or the strong segregation regime of microphase segregation.

There are two key parameters which effectively characterize the observed microphase separated domains. The first is the domain spacing, D, characterizing the periodicity of the underyling lattice. The second is the interfacial width, σ_0, which describes the concentration gradient across a domain boundary. With these parameters one can describe the spatial density profile, the hallmark of the differing regimes of microphase separation. A weakly varying, nearly sinusoidal, spatial density profile characterizes a system in the weak segregation regime. This regime is seen for systems quenched just below the microphase separation transition (MST). This behavior is in contrast to that of the highly ordered, sharply defined (small σ_0) domains characterizing the strongly segregated systems, resulting from deep quenches. In this regime the density profile assumes a "square-wave" form. The appropriate quench parameter was found to be χN, with N the total degree of polymerization of the diblock and χ the familiar Flory interaction parameter.[2] With this terminology in hand, we are now in a position to begin considering contributions to the literature. We focus first on theories valid in the strong segregation regime.

In a series of papers, Helfand and Wasserman examined A–B diblock copolymer microphase separation into lamellae,[3] hexagonally-packed cylinders,[4] and spheres on a body-centered-cubic lattice[5] in the limit of strong segregation. Their model was derived from an assumption that the configurational statistics of the component chains reflected Gaussian behavior in the melt. Their resulting free energy consisted of a decomposition of the total free energy into potentials arising from the formation of domains, the creation of surfaces between these domains, and junction point fluctuations within the interphase region.[6]

This linear decomposition of the total free energy was justified by the narrow interphase approximation (NIA) employed by these investigators. This assumption states that the domains are well defined, exhibiting sharp interfaces. This feature is expected in the strong segregation limit. Their formulation, in general, consisted of a self-consistent solution of the diffusion equation for the partition function.[7] Their free energy, in terms of the partition function, was a function of the quench parameter χN, the fractional length of the A block, f ($f = N_A/N$ where N_A is the degree of polymerization of the A-block), and the bulk densities of the A and B components. They evaluated their free energy expression for the set of ordered morphologies mentioned above.

They obtained a phase diagram denoting the stabilities of the ordered morphologies relative to the disordered phase. The strong segregation limits for these structures were also found and are given in Table I. They also determined the scaling law for the dependence of D on N, finding $D \approx N^{0.643}$ for all three morphologies in this regime.

This series was among the first describing the microphase separation of diblocks in the limit of strong segregation and served as a motivating force for later developments described below.

Ohta and Kawasaki[8] employed a somewhat different approach in characterizing this regime. Their free energy consisted of contributions due to short- and long-range interactions present in the system. They anticipate the free energy, in the limit of $T \to 0$, from an electrostatic analog of the problem consisting of uniformly charged domains.[9] The short-range part was formulated in terms of vertex functions (to be described below). This term characterizes the contribution to the potential from the domain walls and is proportional to the total domain wall area. Due to the influence of the domain walls, the long-range part may be described in terms of density–density

† Present address: Department of Materials Science and Engineering, Massachusetts Institute of Technology, Cambridge, MA 02139.

0024-9297/93/2226-3908$04.00/0

Table I. Stability Regions for Various Morphologies As Predicted by the Strong Segregation Theories of Helfand and Wasserman,[6] Semenov,[10] Ohta and Kawasaki,[8] and DFT

	spheres (f)	cylinders (f)	lamellae (f)
Helfand and Wasserman	0.0–0.15	0.15–0.33	0.33–0.50
Semenov	0.0–0.12	0.12–0.28	0.28–0.50
Ohta and Kawasaki	0.0–0.215	0.215–0.355	0.355–0.50
DFT	0.0–0.195	0.195–0.345	0.345–0.50

correlation functions, $\langle\psi(\mathbf{r})\psi(\mathbf{r}')\rangle$, with $\psi(\mathbf{r})$ the order parameter at space point $\mathbf{r}$ of the microphase-separated system. These correlation functions exhibit a characteristic $1/r$ dependence. It is the "Coulombic" nature of these correlation functions which allows an "electrostatic" formulation of the problem. (More will be said on vertex functions and order parameters below.) A sharp interface and a parameterized density profile are assumed in the solution.

They predict that $D \approx \chi^{1/6}N^{2/3}$ and $\sigma_0 \approx \chi^{-1/2}$ for this regime. We note that their prediction of $D \approx N^{2/3}$ is in good agreement with the prediction of Helfand and Wasserman stated above. They also calculate the strong segregation limits for the lamellar, cylindrical, and spherical morphologies which are given in Table I.

Within the context of micelles, Semenov[10] performed an analysis similar to that of Ohta and Kawasaki. He partitions the total free energy into internal, surface, and external parts. In his "electrostatic" formulation of the problem, the spatial distribution of junction points plays a more important role than in the development of Ohta and Kawasaki. While recovering the predictions of Ohta and Kawasaki for the dependence of D and σ_0 on χN, Table I shows yet another set of strong segregation limits for the lamellar, cylindrical, and spherical microdomains.

We note one feature common to the formalism of these strong segregation theories. This is the linear decomposition of the free energy into separate contributions. This decomposition, in all cases, is facilitated by the assumption of a *narrow* interphase characterizing the segment density profile. Having addressed developments concerning the limit of strong segregation, we now turn our attention to the weak segregation regime of microphase separation.

The first theory to treat weakly segregated systems is that of Leibler.[11] His mean-field free energy formulation consisted of a fourth-order Landau expansion about its value in the disordered phase[12] in terms of vertex functions containing a suitably defined order parameter. The order parameter $\psi(\mathbf{r})$ is defined as the deviation in the local composition of one component from the spatially averaged composition. The vertex functions, describing the density–density correlations within the melt, contain the physical parameters describing the state of the system, χN and f.

This Landau free energy formulation of Leibler implicitly assumes that there is a critical point analogous to phase transitions in Ising and binary fluid systems.[13]

Leibler evaluated his free energy expression for the lamellar, cylindrical, and spherical microphases, developing a phase diagram valid in the weak segregation regime, very close to the critical point. He finds that the transitions from the homogeneous (disordered) phase to spheres, spheres to cylinders, and cylinders to lamellae are first order when $f \neq 0.5$. A second-order transition from the disordered phase to lamellae is predicted at the critical point for the case of symmetric diblocks ($f = 0.5$, $\chi N = 10.495$).

His solution, specifically the calculation of the vertex functions, is performed within a generalized random-phase approximation (RPA).[14] He used a single harmonic to describe the sinusoidal segment density profile. This harmonic, having characteristic wave vector $\mathbf{k}^*$, is assumed to be temperature independent and characterizes the maximum in the structure factor $S(\mathbf{k}^*)$. Given these assumptions, he finds that $D \approx N^{1/2}$ in this regime. Hence, the configurational statistics of the chains are predicted to reflect Gaussian behavior in this regime.

Fredrickson and Helfand[15] extended Leibler's work to account for concentration fluctuations not considered within a mean-field framework. Using a Hartree-type analysis, they reduced Leibler's free energy into a Brazovskii[16] form, thereby adding self-consistent corrections to the Leibler's mean-field free energy.

In general, they observe that the order–disorder transition is weakly first order at $f = 0.5$, exhibiting a characteristic molecular weight dependence: $\chi N = 10.495 + 41.022N^{-1/3}$. Also they observe compositional "windows" in their phase diagram, which allow transitions from the disordered phase to *any* of the three ordered morphologies considered. They further note that Leibler's predictions are recovered when $N \to \infty$, where mean-field behavior is expected since composition fluctuations will be suppressed in this limit.

We note that the evaluation of the higher order vertex functions in this development is performed using the local approximation.[8] Recently, Mayes and Olvera de la Cruz[17] reevaluated Fredrickson and Helfand's free energy with consideration of the angle-dependent higher order vertex functions in their Hartree approximation and found $\chi N = 10.495 + 39.053N^{-1/3}$ at $f = 0.5$.

In another paper by these investigators, the free energy of Leibler was reevaluated using four composition harmonics, instead of only one.[18] They employed nonlocal higher order vertex functions and found, upon minimization of their free energy, that $\mathbf{k}^*$ is temperature dependent. Their calculations for the lamellar and hexagonal morphologies predict a curious result, $D \approx N$ in the weak segregation regime. This is quite different than the prediction of Leibler showing $D \approx N^{1/2}$.

We observe that the weak segregation theories presented have a Landau-type formulation in common. However, comparison of the methods of evaluation of the attendant vertex functions, local versus nonlocal, leads to strongly disparate predictions for the scaling behavior when $D \approx N^{\alpha}$ is considered.

Thus far we have presented theories with predictions valid in either the weak or strong segregation regime of microphase separation. Melenkevitz and Muthukumar[19] performed the first analysis of microphase separation of diblock copolymers focusing on *intermediate* degrees of segregation. Their density functional theory (DFT) is an adaptation of the analyses describing the freezing of simple liquids.[20-22] Melenkevitz and Muthukumar generalized their formalism for liquids comprised of block copolymers. Employing the field-theoretic techniques of Leibler they characterized the dependence of D on χN for the lamellar microphase at *all* degrees of microphase separation, recovering the weak segregation predictions of Leibler and the strong segregation predictions stated above.

Since the publication of Melenkevitz and Muthukumar's work, there have been two studies which address microphase separation of diblock copolymers at all degrees of segregation. Shull[23] considered the behavior of the segment density profile at the interface separating the A-rich and B-rich domains of lamellar structures. He modeled his theory in the spirit of characterizing lamellae present in the bulk, at surfaces, and comprising thin films. His mean-field approach focused on determining the probability distribution functions $q(i,j)$ which are related to the probability of finding the termination of a chain segment of length j within layer i of the lamellar registry. Within the context of appropriately defined boundary

conditions, the self-consistent formalism similar to that of Helfand[7] was used to solve the coupled set of equations for the density profile at the interface and the probability distributions $q(i,j)$.

For a symmetric A–B diblock copolymer, he predicts that the density profile assumes a hyperbolic tangent functional form across the interface when $\chi N > 20$. He observes this because the NIA was not employed in his model. Further, he observes strong segregation behavior for $45 < \chi N \leq 150$ finding that $D \approx \chi^{0.17}N^{0.67}$ in this range of χN. Notably, as χN is decreased, he finds that $D \approx N^{0.95}$ in the region $10.5 \leq \chi N < 15$, similar to the results obtained by Mayes and Olvera de la Cruz.[18] A smooth and rapid transition from $D \approx N^{0.95}$ to $D \approx N^{0.67}$ is seen as χN is increased from 15 to 45.

Vavasour and Whitmore[24] employ a self-consistent mean-field approach very similar to that used by Shull. However, a more general version is employed which allows a solution to the distribution functions describing the configurational statistics of the chains not only in lamellar but also in cylindrical and spherical geometries. For weakly segregated systems, their phase diagram shows a transition to lamellae for symmetric diblocks with an apparent critical point at $\chi N = 10.5$, in agreement with Leibler. However, for asymmetric diblocks, the MST is shifted to *lower* values of χN than that predicted by Leibler, with this downward shift becoming more severe with increasing compositional asymmetry. The transitions between the various morphologies exhibit a smooth but rapid upturn to strong segregation limits as the system becomes deeply quenched. Their predicted strong segregation limits are in good agreement with those predicted by Helfand and Wasserman (see Table I).

They predict $D \approx \chi^p N^q$, $q = p + 1/2$, for all morphologies at all degrees of segregation. At deep quenches they observe $p = 0.2$, $q = 0.7$ for the three morphologies studied, consistent with strong segregation predictions for these exponents. For shallow quenches near the MST, they generally observe an increase in p and q for the lamellar and cylindrical morphologies. For symmetric, lamellae-forming diblocks they predict that $p = 0.5$ and $q = 1$, in good agreement with Shull. For systems forming stable cylinders the increase was not so large, with $p = 0.4$ and $q = 0.9$. No detectable increases in p and q above their strong segregation values was predicted for sphere-forming systems.

Our objective here is to extend the work of Melenkevitz and Muthukumar by similarly studying the cylindrical and spherical morphologies and developing a phase diagram valid at *all* degrees of microphase separation. Throughout our discussions we will focus on the behavior seen at *intermediate* degrees of segregation, providing physical motivation for our observations.

Having introduced the problem at hand, the rest of this paper is organized as follows. We will first outline the formalism relevant to our study of microphase separation of A–B diblock systems and then discuss the minimization procedure needed for the development of the phase diagram. Following this, we will present the calculated phase diagram and examine the dependence of D and σ_o on the quench parameter, χN, for the microphases considered. Finally, we conclude by discussing the implications of work, indicating the directions of future study.

Theory

In this section we sketch the details of DFT needed to give the operative forms of our thermodynamic functionals. The reader is directed to the original development for a thorough discussion of the formalism outlined here.[19]

Our system consists of Gaussian, monodisperse, A–B diblock copolymers composed of N statistical segments. We further assume that both blocks of the copolymer are noncrystallizable and have equal segment lengths and segment volumes. The grand potential, Ω, is then a functional of the spatial variables $\rho(\boldsymbol{r})$ and $\rho_A(\boldsymbol{r})$:

$$\Omega[\rho(\boldsymbol{r}),\rho_A(\boldsymbol{r})] = F[\rho(\boldsymbol{r}),\rho_A(\boldsymbol{r})] - \frac{\mu}{N}\int d\boldsymbol{r}\rho(\boldsymbol{r}) \quad (1)$$

Here, $\rho(\boldsymbol{r})$ and $\rho_A(\boldsymbol{r})$ are the total and A (minority) component segment density variables at $\boldsymbol{r}$. The grand potential functional is formulated in the usual way from the difference between the Helmholtz free energy, F, and the Gibbs function containing the chemical potential μ.

We now assume incompressibility, i.e., $\rho(\boldsymbol{r}) = \rho$, and determine the Helmholtz free energy of the ordered state, $F[\rho_A(\boldsymbol{r})]$, as a functional Taylor series expansion in $\rho_A(\boldsymbol{r})$ about its value in the disordered state, $F[\rho_{Ad}]$:

$$F[\rho_A(\boldsymbol{r})] = F[\rho_{Ad}] + \int d\boldsymbol{r}\left.\frac{\delta F}{\delta\rho_A(\boldsymbol{r})}\right|_{\rho_{Ad}}[\rho_A(\boldsymbol{r}) - \rho_{Ad}] + \frac{1}{2}\int d\boldsymbol{r}d\boldsymbol{r}'\left.\frac{\delta^2 F}{\delta\rho_A(\boldsymbol{r})\delta\rho_A(\boldsymbol{r}')}\right|_{\rho_{Ad}}[\rho_A(\boldsymbol{r}) - \rho_{Ad}][\rho_A(\boldsymbol{r}') - \rho_{Ad}] + \ldots \quad (2)$$

ρ_{Ad} is the A component density in the homogeneous phase. The symbol $\delta/\delta\rho_A(\boldsymbol{r})$ denotes functional differentiation with respect to $\rho_A(\boldsymbol{r})$. We determine F in the disordered state through a fourth-order Landau expansion in the density variable $\rho_A(\boldsymbol{r})$ in terms of the vertex functions Γ_2, Γ_3, and Γ_4[11]

$$F[\rho_A(\boldsymbol{r})] = \frac{kT}{2\rho V}\sum_{k=0}\Gamma_2(\boldsymbol{k},-\boldsymbol{k})\rho_A(\boldsymbol{k})\rho_A(-\boldsymbol{k}) + \frac{kT}{6\rho^2V^2}\sum_{k_1}\sum_{k_2}\Gamma_3(\boldsymbol{k}_1,\boldsymbol{k}_2,-\boldsymbol{k}_1-\boldsymbol{k}_2)\rho_A(\boldsymbol{k}_1)\rho_A(\boldsymbol{k}_2)\rho_A(-\boldsymbol{k}_1-\boldsymbol{k}_2) + \frac{kT}{24\rho^3V^3}\sum_{k_1}\sum_{k_2}\sum_{k_3}\Gamma_4(\boldsymbol{k}_1,\boldsymbol{k}_2,\boldsymbol{k}_3,-\boldsymbol{k}_1-\boldsymbol{k}_2-\boldsymbol{k}_3)\times\rho_A(\boldsymbol{k}_1)\rho_A(\boldsymbol{k}_2)\rho_A(\boldsymbol{k}_3)\rho_A(-\boldsymbol{k}_1-\boldsymbol{k}_2-\boldsymbol{k}_3) + \ldots \quad (3)$$

with

$$\rho_A(\boldsymbol{k}) = \int d\boldsymbol{r}e^{i\boldsymbol{k}\boldsymbol{r}}\rho_A(\boldsymbol{r}) \quad (4)$$

where kT is the Boltzmann constant multiplied by the absolute temperature and V the volume of the system. F is calculated by summing over the contributions of all $\boldsymbol{k}$, thereby accounting for all modes comprising the density profile. This is contrasted with the procedure used in the weak segregation theories in which F is evaluated at a single $|\boldsymbol{k}| = k^*$, the maximum in the structure factor, $S(\boldsymbol{k}^*)$. It is this summation over all modes which allows calculation of the thermodynamics of microphase separation at all degrees of segregation.

In general, the vertex functions are calculated within the random-phase approximation (RPA).[11,14] Γ_2 is the inverse of the structure factor, $S^{-1}(\boldsymbol{k})$, and is given through

$$N\Gamma_2(\boldsymbol{k},-\boldsymbol{k}) = \frac{g(1,x)}{2g(f,x)g(1-f) - \frac{1}{2}[g(1,x) - g(f,x) - g(1-f,x)]^2} - 2\chi N \quad (5)$$

where $g(f,x)$ is the familiar Debye function, $g(f,x) = x^{-2}[e^{-fx} - 1 + fx]$, $x = (kR_g/D)^2$, and f is the fraction of the A component in the diblock copolymer. Note that in the definition of x, $\boldsymbol{k}$ is dimensionless. Minimization of the free energy with respect to x will determine the periodicity, D, of the domains. We will see that the quench parameter,

χN, appears only in the expression for $N\Gamma_2$. This will simplify the minimization problem when deep quenches are studied (see below).

The higher order vertex functions are taken as constants with

$$N\Gamma_3(\boldsymbol{k}_1, \boldsymbol{k}_2, -\boldsymbol{k}_1, -\boldsymbol{k}_2) = N\Gamma_3(1) \quad (6)$$

$$N\Gamma_4(\boldsymbol{k}_1, \boldsymbol{k}_2, \boldsymbol{k}_3, -\boldsymbol{k}_1, -\boldsymbol{k}_2, -\boldsymbol{k}_3) = N\Gamma_4(0,0) \quad (7)$$

where $N\Gamma_3(1)$ and $N\Gamma_4(0,0)$ are defined by Leibler.[11] Here we have employed the local approximation,[8] which has been used in theories addressing both weakly[15] and strongly[8] segregated systems.

Since we expect the ordered phase to be periodic in space, it is convenient to express the density profile $\rho_A(\boldsymbol{r})$ in terms of a Fourier series:

$$\rho_A(\boldsymbol{r}) = \rho f(\boldsymbol{r}) = \rho f + \rho \sum_{k_n \neq 0} \{a_n \cos(\boldsymbol{k}_n \boldsymbol{r}) + b_n \sin(\boldsymbol{k}_n \boldsymbol{r})\} \quad (8)$$

The set of reciprocal lattice vectors $\{\boldsymbol{k}_n\}$ will define the morphology investigated. The sets of Fourier coefficients, $\{a_n\}$ and $\{b_n\}$, become the order parameters of the theory.

When the condition for an extremum in Ω is imposed

$$\left.\frac{\delta\Omega[\rho_A(\boldsymbol{r})]}{\delta\rho_A(\boldsymbol{r})}\right|_{\rho Ao(\boldsymbol{r})} = 0 \quad (9)$$

with $\rho_{Ao}(\boldsymbol{r})$ the A component segment density profile which extremizes the grand potential, we arrive at the final form for the difference in grand potential, $\Delta\Omega$, between that of the ordered, Ω_o, and disordered, Ω_d, states:

$$\Delta\Omega = \frac{N(\Omega_o - \Omega_d)}{kT\rho_d V} = -\frac{N}{4}\sum_{k_n \neq -k_n \neq 0} \Gamma_2(\boldsymbol{k}_n)(a_n^2 + b_n^2) + \frac{N\Gamma_3(1)}{8}\sum_{k_n}\sum_{k_m}(a_n a_m a_{n+m} + 2a_n b_m b_{n+m} - b_n b_m b_{n+m}) + \frac{N\Gamma_4(0,0)}{192}\sum_{k_n}\sum_{k_m}\sum_{k_l}(4a_n a_m a_l a_{n+m+l} + 3a_n a_m a_l a_{n+m-m} - 4b_n b_m b_l b_{n+m+l} + 3b_n b_m b_l b_{m+l-n} - 12b_n b_m a_l a_{n+m+l} + 12a_n a_m b_l b_{n+m+l} + 12a_n a_m b_l b_{m+l-n} - 6a_n a_m b_l b_{n+m-l}) + \ldots \quad (10)$$

We see that $\Delta\Omega$ is a function of f (appearing through the vertex functions and the Fourier series for $\rho_A(\boldsymbol{r})$), χN, and R_g/D (appearing in $N\Gamma_2$), $\{\boldsymbol{k}_n\}$ (the morphology), and the order parameters $\{a_n\}$ and $\{b_n\}$.

Having obtained the operative form of our free energy, we now discuss the minimization procedure in the next section.

Minimization Technique

Calculation of the minimum $\Delta\Omega$ for a particular set of conditions (f, χN, and $\{\boldsymbol{k}_n\}$) presents a variational problem in $2n + 1$ parameters ($\{a_n\}$, $\{b_n\}$, R_g/D). n becomes very large as the degree of quench is increased, making the solution a formidable task. Therefore, we parameterize the expected density profiles in order to alleviate the computational difficulty associated with such a multivariable minimization problem. We have exploited the symmetries of the microphases considered here (lamellae, cylinders, and spheres) and have developed expressions for the density profiles in terms of f, $\{\boldsymbol{k}_n\}$, and σ_o, the interfacial width.

Melenkevitz and Muthukumar have used

$$a_m = 2fj_0\left(\frac{1}{2}fk_m\right)\exp\left[-\frac{1}{2}k_m^2\left(\frac{\sigma_o}{D}\right)^2\right] \quad (11)$$

with j_0 a spherical Bessel function of order zero for the order parameters describing the lamellar morphology. They have shown that this parameterization successfully characterizes the behavior of the segment density profile at *all* degrees of microphase separation.[19]

We now introduce similar density parameterizations for hexagonally-packed cylinders

$$a_m = \left(\frac{32\pi}{\sqrt{3}}f\right)^{1/2}\frac{J_1\left(\left[\frac{\sqrt{3}}{2\pi}f\right]^{1/2}k_m\right)}{k_m}\exp\left[-\frac{1}{2}k_m^2\left(\frac{\sigma_o}{D}\right)^2\right] \quad (12)$$

and body-centered-cubic spheres

$$a_m = 4(9\pi f^2)^{1/3}\frac{j_1\left(\left[\frac{3}{8\pi}f\right]^{1/3}k_m\right)}{k_m}\exp\left[-\frac{1}{2}k_m^2\left(\frac{\sigma_o}{D}\right)^2\right] \quad (13)$$

where J_1 and j_1 are Bessel and spherical Besel functions of order one, respectively. Since the symemtry of these structures allows a half-interval Fourier representation, $\{b_n\} = 0$ for all the morphologies considered here. $\{\boldsymbol{k}_n\}$ for each morphology is found from the primitive translation vectors of the underyling lattice.[25] Using the technique of parameterization, the evaluation of the minimum $\Delta\Omega$ has been reduced to a two-variable, R_g/D and σ_o/D, variational problem.

The minimization of $\Delta\Omega$ proceeds as follows. Given the set of parameters: f, χN, and $\{\boldsymbol{k}_n\}$, the expression for $\Delta\Omega$ is minimized with respect to R_g/D and σ_o/D. Then, the system is characterized according to the following set of stability criteria: If $\Delta\Omega > 0$ the disordered phase is stable. If $\Delta\Omega = 0$ the order–disorder transition occurs, and if $\Delta\Omega < 0$ the ordered phase is stable. The ordered phase characterizing the morphology is the one yielding the *lowest* value for $\Delta\Omega$.

Having sketched the theory describing the thermodynamics of our diblock copolymer systems and detailing our minimization procedure, we now present the results of our study.

Results and Discussion

In Figure 1 we consider the predicted phase diagram. Part a shows the regions of stability for lamellae (LAM), hexagonally-packed cylinders (CYL), and body-centered-cubic spheres (SPH). The location of the homogeneous, disordered (DIS) phase is also indicated. Since the phase diagram is symmetric about $f = 0.50$ for the diblock system, we concentrate on the left half and consider $0.10 \leq f \leq 0.50$. For $\chi N \leq 55$ we present the DIS-SPH (▲), SPH-CYL (■, □), and CYL-LAM (●, ○) transitions. We have also calculated the strong segregation limits for spheres ($f = 0.195$) and cylinders ($f = 0.345$) at $\chi N = 300$ (see the last entry in Table I). We will show that at $\chi N = 300$ the domains of these morphologies are strongly segregated. These strong segregation limits compare favorably with those of Ohta and Kawasaki quoted in the table. We attribute the slight discrepancies observed between the predictions of DFT and Ohta and Kawasaki for these limits to the differences in the evaluation of term containing $N\Gamma_2$. We have *explicitly* calculated the wave vector dependence of this term, while Ohta and Kawasaki employ an approximate, bilinear form for $N\Gamma_2$ in order to facilitate an analytical solution.[8]

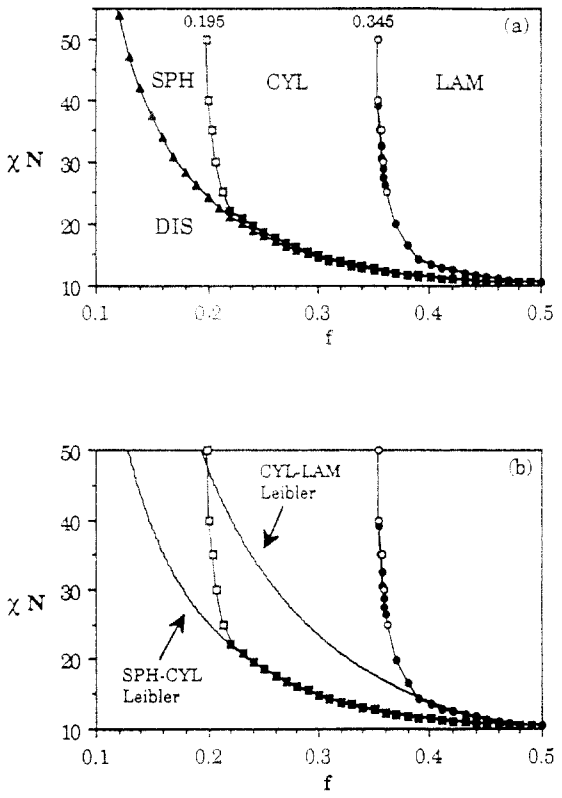

Figure 1. Part a: phase diagram as predicted by DFT. The strong segregation limits (in terms of f) for spheres and cylinders are indicated at the top of the phase diagram. Part b: comparison of the phase diagrams of DFT and Leibler. See text for an explanation of the plotting symbols.

In part b we show the depatures of the SPH-CYL and CYL-LAM transitions as calculated by DFT from the predictions of the weak segregation theory of Leibler. We see that at $\chi N \approx 15$ the CYL-LAM transition calculated by DFT *sharply* deviates from the weak segregation prediction, with a rapid approach to a strong segregation limit for this transition as χN is further increased. Similar behavior is seen for the SPH-CYL transition beginning at $\chi N \approx 20$. Note that this rapid approach of the SPH-CYL and CYL-LAM transitions to their strong segregation limits was also observed by Vavasour and Whitmore.[24] For the range of f studied, the DIS-SPH transition shows no differences from the predictions of Leibler. Comparison of the predictions of DFT with those of the Leiblers theory (using the local approximation for the higher order vertex functions) enables one to determine its region of applicability.

We have used both shaded and unshaded plotting symbols to construct these curves. The data shown with filled plotting symbols (●, ■, ▲) were obtained using the expression for $\Delta\Omega$ given in eq 10, which we will term the "full" theory. Data indicated by unshaded symbols (○, □) were calculated using only the first term of eq 10, i.e., the term containing $N\Gamma_2$. This simplification of the theory was necessary in order to carry out the calculations of the SPH-CYL transition for $\chi N > 20$ and to investigate the intermediate-strong segregation behavior for the cylindrical and spherical microphases.

In the previous section we noted that calculation of $\Delta\Omega$ involves a summation over all $\boldsymbol{k}_n$. As the degree of quench is increased the density profile assumes a "square-wave" appearance. Consequently, many wave vectors (of order 10^4) are needed to yield a convergent Fourier expansion for $\rho_A(\boldsymbol{r})$. The calculation of the second and third terms of eq 10 for such a large set of wave vectors is beyond the limits of the available computational resources. Figure 2 shows the percent deviation of $\Delta\Omega$ calculated using the truncated expression from its value using the "full" theory. (The deviation is negative because, in general, the second- and third-order terms are negative, and the fourth-order term is positive and has higher magnitude than the third.) Fortunately, for large enough χN, the first term in eq 10 comprises over 99% of $\Delta\Omega$, making the truncation of $\Delta\Omega$ to this single term a reasonable approximation. The success of this approximation is seen when the CYL-LAM transition is calculated using the full (●) and the truncated (○) versions of eq 10 for $25 \leq \chi N \leq 40$. The curves are virtually identical for this region of χN. This is not too surprising in that as the degree of quench of the system increases (i.e., as temperature is decreased), the terms in the theory dependent on enthalpic interactions begin to play a dominant role in the thermodynamics. In fact, for deeply quenched systems, these terms become the overriding factor in the free energy. Since χN, a pairwise interaction parameter, appears *only* in $N\Gamma_2$, this term would be expected to characterize the thermodynamics of the system as it is quenched deeply into the microphase separated region of the phase diagram. Therefore, we are confident that this approximate form of $\Delta\Omega$ captures the essential physics of the full theory when deeply quenched systems are investigated.

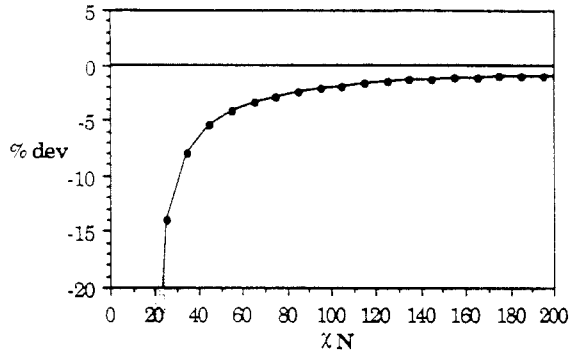

Figure 2. Percent deviation of the value of $\Delta\Omega$ found from the truncated free energy expression from its value determined by the "full" fourth-order expression. The calculation is performed for lamellar microdomains at $f = 0.45$ (●).

We now turn our attention to the characterization of the dependence of D and σ_0 on χ and N for the morphologies considered. In part a of Figure 3 we investigate the dependence of D on N from a plot of ln (D/R_g) versus lin (χN) for the lamellar morphology. This is done for $f = 0.50$,[19] 0.45, and 0.40. We see the regions of weak $D \approx N^{0.50}$ ($R_g \approx N^{1/2}$) and strong $D \approx N^{0.67}$ segregation behaviors. Between these regions we see $D \approx N^{0.72}$ with 0.72 an "effective" exponent characterizing the crossover behavior between the limiting regimes. This region, the "intermediate" segregation regime, will be further discussed below. (The uncertainty in the exponents calculated in this study is approximately ±0.01.) We see that these exponents are independent of the value of f, consistent with predictions for the weak and strong segregation regimes. The locations of the changes in these exponents allow one to delineate the ranges of χN corresponding to differing degrees of segregation. For example, for $f = 0.40$, we see weak segregation when $11.32 \leq \chi N < 14.0$, intermediate segregation when $14.0 \leq \chi N \lesssim 100$, and strong segregation when $\chi N \gtrsim 100$.

Part b of Figure 3 shows a plot of ln (σ_0/D) versus ln (χN) for $f = 0.50$,[19] 0.45, and 0.40. We see a non-universal dependence of σ_0 on χ and N at weak and intermediate degrees of segregation. However at $\chi N \gtrsim 100$ we recover the strong segregation behavior, $\sigma_0 \approx \chi^{-0.50}$. Finally, we note that the full expression for $\Delta\Omega$ was used in determining these curves.

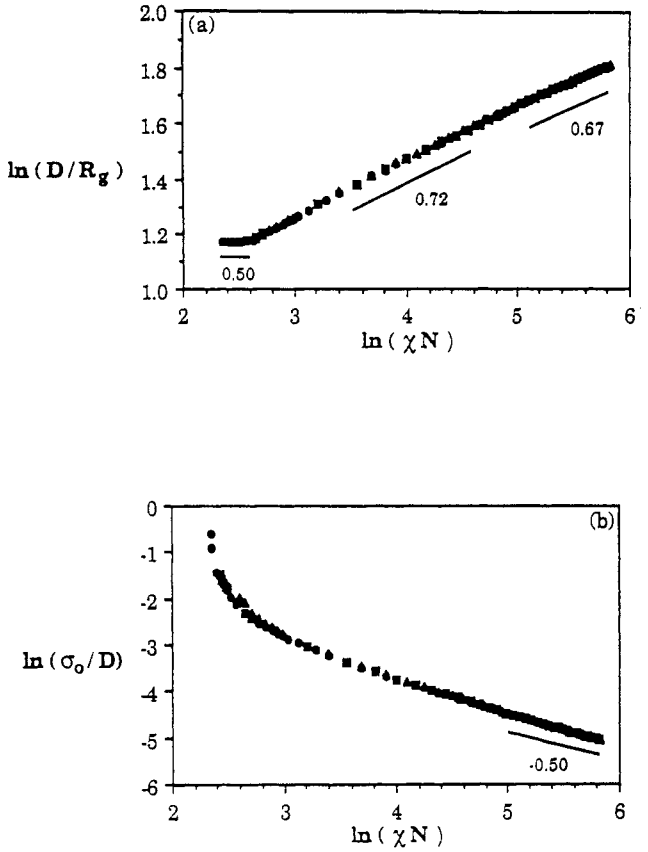

Figure 3. Characterization of the dependence of the domain spacing, D (part a), and the interfacial width, σ_0 (part b), on χ and N for lamellae at $f = 0.50$ (●), 0.45 (■), and 0.40 (▲). The values adjacent to the lines in part a indicate the value of α in $D \sim N^{\alpha}$. That in part b indicates the value of β in $\sigma_0 \approx \chi^{\beta}$.

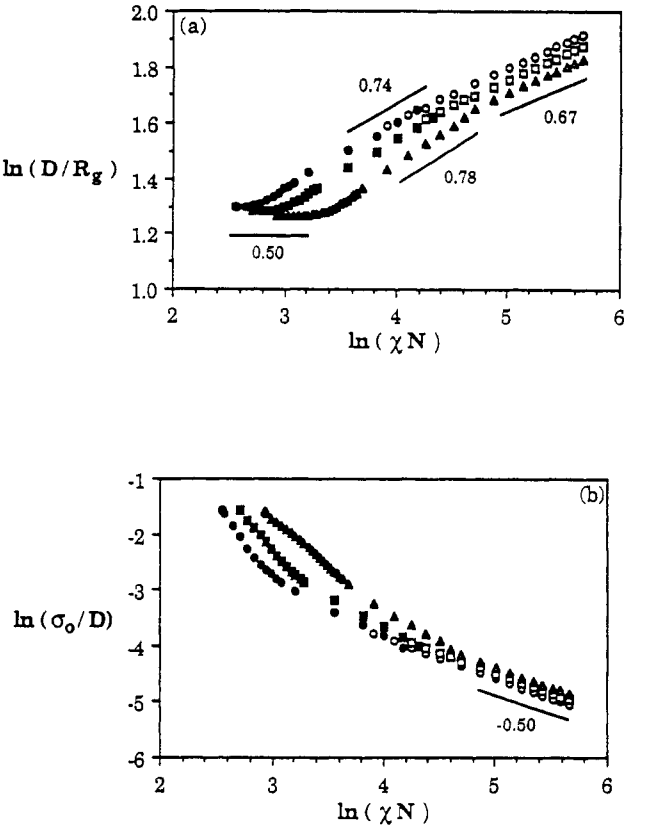

Figure 4. Characterization of the dependence of the domain spacing, D (part a), and the interfacial width, σ_0 (part b), on χ and N for cylinders at $f = 0.35$ (●, ○), 0.30 (■, □), and 0.25 (▲, △). The values adjacent to the lines in part a indicate the value of α in $D \sim N^{\alpha}$. That in part b indicates the value of β in $\sigma_0 \approx \chi^{\beta}$. The shade of the plotting symbols indicates the regions where the full and truncated versions of the free energy are used (see text).

Figure 4 similarly characterizes D and σ_0 for the cylindrical microdomains. In part a we see the weak ($D \approx N^{0.50}$) and strong ($D \approx N^{0.67}$) segregation regions, with exponents independent of f. Between these limiting regimes we see intermediate segregation exhibiting an f-dependent exponent with values ranging from 0.74 when $f = 0.35$ to 0.78 when $f = 0.25$. In characterizing the interfacial width, part b of Figure 4, we observe similar transition from nonuniversal behavior in the weak and intermediate segregation regimes to the universal strong segregation law $\sigma_0 \approx \chi^{-0.50}$ as χN is increased. Note that the truncated expression of $\Delta\Omega$ was needed in order to investigate the strong segregation regime for cylinders.

Similarly, we characterize the spherical microdomain in Figure 5 for $f = 0.19$. Again, in part a, we see the three regimes described above when we consider the dependence of D on N. Here we observe $D \approx N^{0.82}$ at intermediate degrees of segregation. The dependence of σ_0 on χN shown in part b exhibits similar behavior to that of the lamellar and cylindrical microphases. Unfortunately, due to the extreme demand placed on the available computational resources for this calculation, a complete set of data is unobtainable at this time. We have only included on Figure 5 data in which the Fourier expansion describing the A component segment density profile, eq 8, is fully converged. We merely quote the apparent exponent 0.82 in the beginning of the intermediate segregation regime to give an *indication* of the degree of chain deformation expected for this morphology. Additionally, despite using the truncated expression for $\Delta\Omega$, further computational difficulties exist which limit study of only one value of f. Therefore, no comment may be made at this time regarding the dependence of this intermediate exponent on f.

Finally, we depict "micrographs" of the cylindrical microdomains at various degrees of segregation. Here we investigate the ability of the density parameterization to render effectively the physical details of a given morphology. The images are constructed from specifying f, $\{k_n\}$, and σ_0/D in eqs 8 and 12. Black regions indicate pure A component ($f = 1.0$), and white regions are pure B component ($f = 0.0$).

Figure 6 shows images of hexagonally-packed cylinders (axial projection) at $f = 0.30$ for $\sigma_0/D = 0.25$ (top), 0.10 (middle), and 0.01 (bottom), with D arbitrary and constant. We note the sharpening of the domain structure as the interfacial width becomes narrower. The value of $\sigma_0/D = 0.25$ in part a of Figure 6 is typical of a late-weak to early-intermediate degree of segregation. $\sigma_0/D = 0.10$ in part b is characteristic of the intermediate segregation regime while $\sigma_0/D = 0.01$ in part c describes strongly segregated microdomains. Similar "micrographs" for other morphologies can readily be constructed.

We now discuss the physical reasons for the presence of an intermediate segregation regime through the dependence of the molecular weight exponent in the scaling law for D, on the choice of morphology and f. As the system becomes deeply quenched the junction points undergo "localization".[19] The extreme situation exists when the junction points lie on the surface of the domain, yielding strongly segregated domains. Thus, the domain and surrounding material are pure and the interfacial width is very small. A–B interactions occur only at the interface. The opposite case is seen in the weak segregation region of the phase diagram. A very weak periodicity exists in the system, with a broad dispersion of junction points characterizing the interfacial region. Starting from this point, as the system is further quenched into the intermediate segregation regime, the chains are stretched in

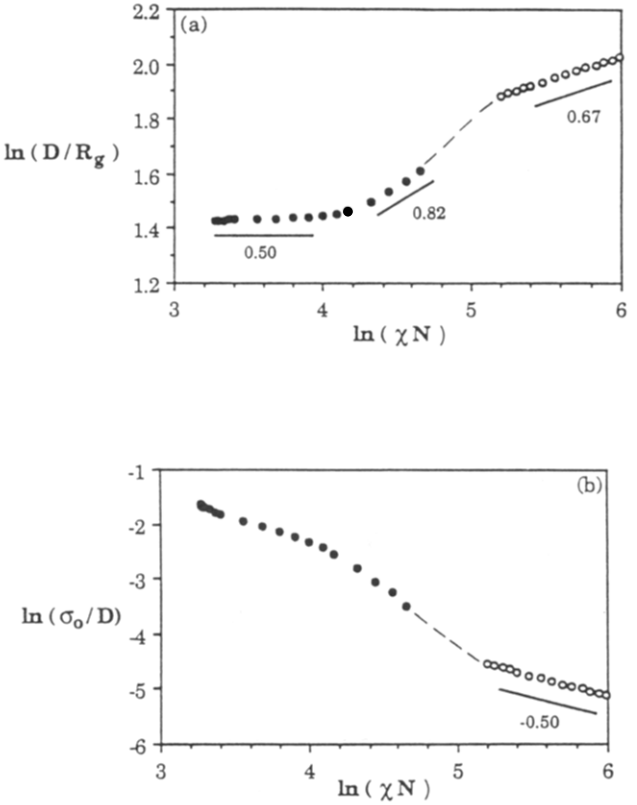

Figure 5. Characterization of the dependence of the domain spacing, D (part a), and the interfacial width, σ_o (part b), on χ and N for spheres at $f = 0.19$ (●, ○). The values adjacent to the lines in part a indicate the value of α in $D \simeq N^{\alpha}$. That in part b indicates the values of β in $\sigma_o \approx \chi^{\beta}$. The shade of the plotting symbol indicates the regions where the full and truncated versions of the free energy are used (see text).

order to localize the junctions. Since the junctions are not completely localized, a significant number of A–B contacts exist which further contribute to chain stretching.

The degree of stretching in this regime will also depend on the mean curvature and complexity of the domain structure considered. The lamellar morphology, exhibiting one-dimensional periodicity, has an infinite principal radius of curvature regardless of the value of f. Hence, no dependence of the intermediate exponent on f is expected from this effect. However, the cylindrical morphology which is periodic in two dimensions has an f-dependent principal radius of curvature, decreasing as f is decreased. This causes the A and B blocks to be stretched asymmetrically, allowing for more A–B contacts in the interfacial region as f is decreased.[26] On the basis of these arguments the spherical morphology, which is periodic in three dimensions and has two principal radii of curvature, should exhibit even stronger chain stretching in this regime.

Conclusions

In this study we have investigated microphase separation of diblock copolymers through calculation of the phase diagram and the morphological characteristics for three ordered microphases: lamellae, hexagonally-packed cylinders, and body-centered-cubic spheres. A general scheme was implemented which allowed study of diblock copolymers at all degrees of segregation. We have reproduced the behavior seen in the weak and strong segregation regimes by comparing our predictions for these regimes to those of established theories. An intermediate segregation regime emerged between these limiting cases and exhibited unique properties due to the phenomenon of localization. We focused on the scaling relationship D

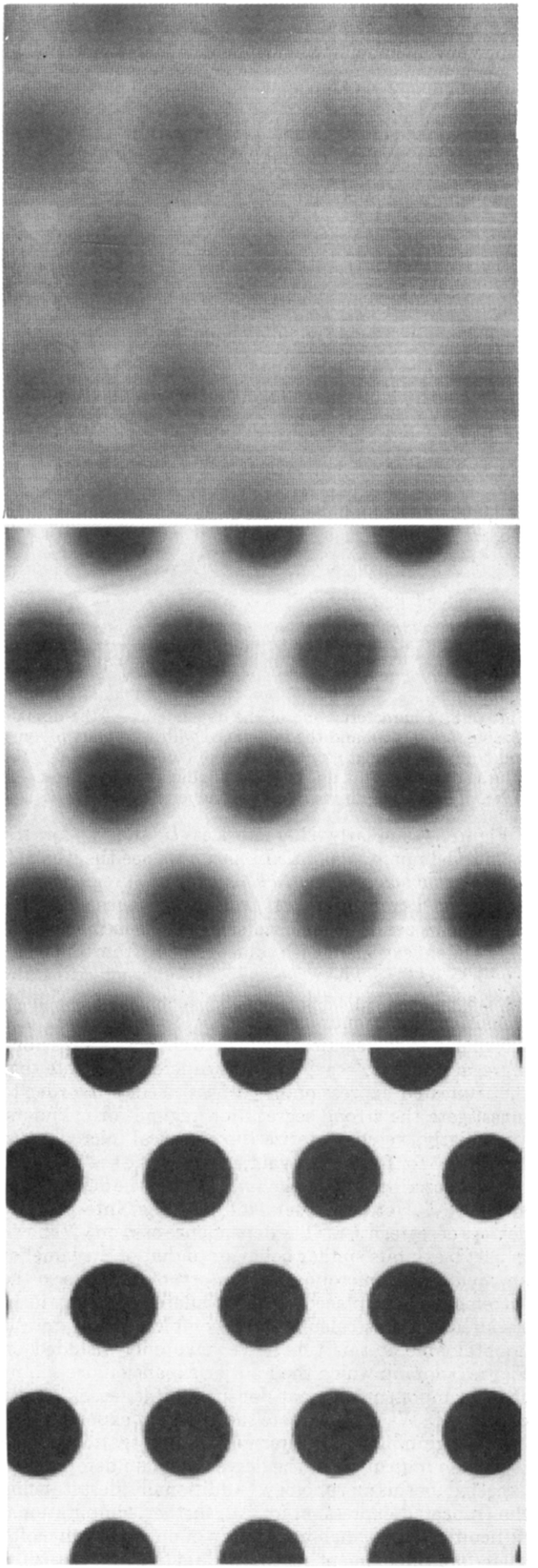

Figure 6. Images of hexagonally-packed cylinders (axial projection) for $f = 0.30$ at $\sigma_o/D = 0.25$ (top), 0.10 (middle), and 0.01 (bottom).

$\approx N^{\alpha}$ and observed that α depends both on the choice of morphology and f, which is not seen in the weak or strong segregation limits. Finally, we have shown that density profile parameterization greatly reduces the technical complexity inherent in this calculation. Further, no physical details of the microstructures were lost when their density profile assumed a parameterized form.

Comparing our results with those Mayes and Olvera de la Cruz[18] and the self-consistent field treatments of Shull[23] and Vavasour and Whitmore,[24] we see that the primary difference is the scaling exponent α in the weak segregation regime. The value of this exponent, in a sense, arises from a question of convergence. That is, when our development and that of Mayes and Olvera de la Cruz are compared, the difference lies in the vertex functions employed: local versus non-local. Since the predictions of Leibler for the weak segregation regime are recovered in our development we naturally expect that the consideration of nonlocal higher order vertex functions would yield results similar to those of Mayes and Olver ade la Cruz. However, we are at present unable to obtain reliable predictions from DFT when considering nonlocal higher order vertex functions—particularly for the cylindrical and spherical microphases—due to the very large number of wave vectors needed for a convergent Fourier series.

Although not as obvious, this difference is also the source of the discrepancies between our predictions and those of the self-consistent field theories for weakly and intermediately segregated systems.[23,24] We note, however, that these treatments suffer from an inherent technical difficulty. For the case of symmetric diblock copolymers, the amplitude of the density profile and, consequently, the free energy vanish continuously as the MST is approached from the deeply quenched state. Therefore, in these formalisms, it is difficult to ascertain a precise value for the minimum free energy close to the MST. In *both* studies, an extrapolation to Leibler's predictions for the domain spacing at the MST was necessary when addressing weakly segregated symmetric diblocks. Similar numerical problems also existed for asymmetric diblocks, which prevented a precise calculation of the domain spacings of systems close to the MST.[24] This technical problem was the opposite of that experienced in the present study, where approximations were needed to consider strongly segregated systems forming cylindrical and spherical microstructures.

We now comment on the status of experimental work pertinent to the problem addressed here. We focus on the strong segregation limits observed for the morphologies considered in this study and the observed values of α in $D \approx N^{\alpha}$ in the intermediate segregation regime.

Since we did not consider the presence of the ordered-bicontinuous double diamond (OBDD) morphology[27] in our phase diagram, we can only comment on the strong segregation limit for spheres at this time. For polystyrene–polyisoprene diblock copolymers, which are well represented by our development, the strong segregation limit for spheres is experimentally observed to lie at $f \approx 0.18$.[28] This is in excellent agreement with our predicted value of $f = 0.195$ (see Table I). We further note that of the theoretical developments presented here, our predictions compare quite favorably with experimental observations. On the basis of this, we are optimistic that a similar degree of agreement will be see for the strong segregation limits of the cylindrical and the OBDD microphases.

The prediction that α in $D \approx N^{\alpha}$ is higher than that observed in the strong segregation limit as χN is increased from the weak segregation regime was experimentally observed by Almdal and co-workers[29] for symmetric diblocks of poly(ethylenepropylene)–poly(ethylethylene) forming lamellae. They observed the apparent power law, $D \approx N^{0.8}$. Hadziioannou and Skoulios[30] observed a similar exponent (0.79) for their symmetric polystyrene–polyisoprene diblocks. However, in each of these investigations, a crossover from the intermediate to the strong segregation regime was not observed. Assuming, however, that the experimentally observed value of $\alpha = 0.8$ corresponds to the intermediate regime, the difference between 0.8 and 0.72 (predicted by DFT for lamellae) is not unreasonable given that this exponent is nonuniversal and depends on compressibility, chain stiffness, segment volumes, etc. (Melenkevitz and Muthukumar[19] further argue this point.) Experimental determination of α for the cylindrical and spherical microphases in the intermediate segregation regime will further test the predictive power of density functional theory presented here.

We close this section by stating the implications of this work. The scheme described above is general. Analysis of systems exhibiting variations in block copolymer architecture or chemical composition is possible through appropriate modification of the above formalism. For example, modifications in the vertex functions in eq 3 would allow study of the microphase separation of A–B star-diblocks.[31] Compressibility may be reintroduced into the calculation as another variational parameter by retaining the full form of eq 1. The effect of composition fluctuations on the weak segregation behavior can be addressed by incorporation of the techniques introduced by Brazovskii and developed by Fredrickson and Helfand into the free energy functional. Finally the stability of other morphologies such as the ordered-bicontinuous double diamond (OBDD) may be investigated by suitable density parameterization using the proper $\{\boldsymbol{k}_n\}$.

Acknowledgment. R.L.L. acknowledges J. M. Melenkevitz for his contributions during the early stages of this work and for his comments on the manuscript. R.L.L. thanks C. U. Thomas and J. J. Rajasekaran for stimulating discussions and K. G. Koniaris for his assistance in rendering the microphase images. We thank E. L. Thomas and the reviewers for their careful review of the manuscript. This work is supported by NSF Grant DMR-9008192 and the Materials Research Laboratory at the University of Massachusetts at Amherst.

References and Notes

(1) Aggarwal, S. L., Ed. *Block Copolymers*; Plenum: New York, 1970.
(2) Flory, P. J. *Principles of Polymer Chemistry*; Cornell University: Ithaca, 1953.
(3) Helfand, E.; Wasserman, Z. R. *Macromolecules* **1976**, *9*, 879.
(4) Helfand, E.; Wasserman, Z. R. *Macromolecules* **1980**, *13*, 994.
(5) Helfand, E.; Wasserman, Z. R. *Macromolecules* **1978**, *11*, 960.
(6) Helfand, E.; Wasserman, Z. R. *Developments in Block Copolymers*; Goodman, I., Ed.; Elsevier: New York, 1982; Vol. 1.
(7) Helfand, E. *Macromolecules* **1975**, *8*, 552.
(8) Ohta, T.; Kawasaki, K. *Macromolecules* **1986**, *19*, 2621.
(9) Jackson, J. D. *Classical Electrodynamics*; John Wiley and Sons: New York, 1975.
(10) Semenov, A. N. *Sov. Phys.—JETP (Engl. Transl.)* **1985**, *61*, 733.
(11) Leibler, L. *Macromolecules* **1980**, *13*, 1602.
(12) Landau, L. D.; Lifshitz, E. M. *Statistical Physics*; Pergamon Press: Oxford, 1980; Part 1.
(13) Plischke, M.; Bergersen, B. *Equilibrium Statistical Physics*; Prentice Hall: Engelwood Cliffs, 1989.
(14) de Gennes, P.-G. *J. Phys. (Paris)* **1970**, *31*, 235.
(15) Fredrickson, G. H.; Helfand, E. *J. Chem. Phys.* **1987**, *87*, 6.
(16) Brazovskii, S. A. *Sov. Phys.—JETP (Engl. Transl.)* **1979**, *91*, 7228.
(17) Mayes, A. M.; Olvera de la Cruz, M. *J. Chem. Phys.* **1991**, *95*, 4670.
(18) Mayes, A. M.; Olvera de la Cruz, M. *Macromolecules* **1991**, *24*, 3975.

(19) Melenkevitz, J.; Muthukumar, M. *Macromolecules* **1991**, *24*, 4199.
(20) Ramakrishnan, T. R.; Yussouff, M. *Phys. Rev. B* **1977**, *19*, 2775.
(21) Haymet, A. D. J.; Oxtoby, D. *J. Chem. Phys.* **1981**, *74*, 2559.
(22) Haymet, A. D. J. *J. Chem. Phys.* **1983**, *78*, 4641.
(23) Shull, Kenneth R. *Macromolecules* **1992**, *25*, 2122.
(24) Vavasour, J. D.; Whitmore, M. D. Submitted for publication in *Macromolecules*, 1992.
(25) Kittel, C. *Introduction to Solid State Physics*; John Wiley and Sons: New York, 1976.
(26) Ching, E. S. C.; Witten, T. A. *Europhys. Lett.* **1992**, *19*(8), 687.
(27) Thomas, E. L.; Alward, D. B.; Kinning, D. J.; Handlin, D. L.; Fetters, L. J. *Macromolecules* **1986**, *19*, 2197.
(28) Gobran, D. Ph.D. dissertation, University of Massachusetts, 1990.
(29) Almdal, K.; Rosedale, J. H.; Bates, F. S.; Wignall, G. D.; Fredrickson, G. H. *Phys. Rev. Lett.* **1990**, *65*, 1112.
(30) Hadziioannou, G.; Skoulios, A. *Macromolecules* **1982**, *15*, 258.
(31) Olvera de la Cruz, M.; Sanchez, I. C. *Macromolecules* **1986**, *19*, 2501.